

# The Inverse Carson's Equations Problem: Definition, Implementation and Experiments

C. H. Tam, F. Geth, N. Mithulananthan, *Senior Member, IEEE*,

**Abstract**—In recent years, with the increase in renewable energy and storage penetration, power flow studies in low-voltage networks have become of interest in both industry and academia. Many studies use impedance represented by sequence components due to the lack of datasets with fully parameterized impedance matrices. This assumes that the network impedance is balanced, which is typically not the case in the low voltage network and therefore risks the accuracy of the study. This paper proposes a methodology for the recovery of more detailed impedance data from sequence components as an inverse problem, i.e. the inverse Carson's equations problem, for both overhead lines and cables. We consider discrete properties like material and configuration of conductors common in the distribution network and investigate what data can be reliably recovered from only sequence components using nonlinear optimisation models. Presented results include uniqueness of recovered variables and the likelihood of mismatch.

**Index Terms**—Power distribution networks, conductors, Carson's equations, inverse problems, nonlinear optimisation

## I. INTRODUCTION

WITH the proliferation of roof-top photovoltaics, electric vehicles and battery storage systems, concerns have been raised on the operation of (unbalanced) low-voltage (LV) power distribution networks. Power flow simulation is a technique used by utilities to understand and manage the impact of these new energy technologies. One of the obstacles for LV power flow studies is the lack of high-quality network models, which nevertheless are needed for decision-support approaches [1].

### A. Imperfect Network Datasets

Historically, utilities may have calculated the impedance values for a limited set construction codes for overhead lines and cables, based on a number of assumptions such as operational temperature. Further approximations may have been made, e.g. reduction to positive and zero sequence impedance,  $Z_{11}$  and  $Z_{00}$  respectively, to enable entry into legacy engineering software. Information for calculating impedance anew may not be kept properly and makes recovery of full impedance matrices difficult. Projects have been run to release more comprehensive LV network models, such as [2] in Australia and [3] in UK. However, the impedance data is given only in  $Z_{11}$  and  $Z_{00}$ , which assumes balanced network impedance. Such approximation impacts the accuracy of power flow simulation [4]–[6].

### B. Carson's Equations

Impedance of overhead lines and cables are dependent on the environment and installation, due to mutual inductive

effects between conductors and capacitive coupling to earth. Impedance values are established from Maxwell's laws, either solved through finite element simulation or Carson's equations. Carson's equations, an approximation of Maxwell's laws, derive the impedance matrices for electromagnetically coupled conductors based on geometry, material, resistivity of the conductor and the earth, temperature, and cross-section.

### C. Contribution

To enhance the quality of impedance datasets, this paper proposes a methodology to recover the inputs to Carson's equations based on zero and positive sequence components. The contributions are,

- Proposing a methodology to solve the inverse Carson's equations problem, allowing us to recover information such as pole and cable geometry, material, etc based on partial information usually provided from utilities, i.e., diagonal sequence components and indication of being an overhead line or a cable.
- Conducting numerical experiments to validate accuracy, model uncertainty and mismatch risks.

### D. Notation and Preliminaries

To prevent ambiguity, specific terms are defined to distinguish overhead line and cable construction properties. A *conductor* is formed by  $N_f$  strands and it is more specifically referred to as a *wire* for overhead lines and as a *core* for cables. For example, on the left of Fig. 1 is a 4-conductor 19-strand cable and on the right is a 3-wire 7-strand overhead line.

The term *forward calculation* is referred to as having all required information to obtain the reference diagonal sequence components of impedance  $R_{l,00}^{\text{ref}}$ ,  $R_{l,11}^{\text{ref}}$ ,  $X_{l,00}^{\text{ref}}$ ,  $X_{l,11}^{\text{ref}}$ , and that of shunt susceptance  $B_{l,00}^{\text{ref}}$ ,  $B_{l,11}^{\text{ref}}$ . Next, the term *inverse estimation* is referred to as establishing a likely combination to explain the sequence components being given.

### E. Paper Structure

Section II is a literature review on the importance of using accurate LV network impedance, use of Carson's equations in power systems. Section III summarizes how to derive the impedance values for common LV networks configurations through Carson's equations. Section IV defines the mathematical problem statement of the inverse Carson's equations problem, and Section V develops numerical results for 2, 3 and 4-conductor overhead lines and cables. Lastly, Section VI provides conclusions and avenues for future work.

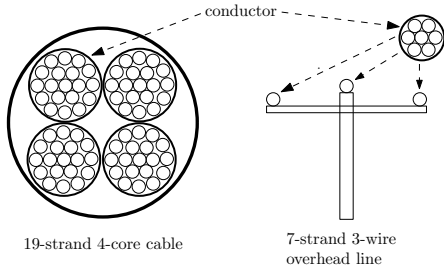


Fig. 1. The left diagram represents a cable with  $N_f=19$  and  $n_f=4$ , on the right an overhead line with  $N_f=7$  and  $n_f=3$ .

## II. LITERATURE STUDY

In forward calculation, the inputs to Carson's equations are taken from standard construction codes. For a 3- or 4-conductor network, sequence components are obtained by forward calculation as depicted in top half of Fig. 2. Carson's equations are used to obtain the series impedance and shunt admittance matrices. For a 4-conductor network, Kron's reduction of impedance matrix and partitioning of admittance matrix are done to reduce the matrix so that symmetric component transformation can be performed to obtain the sequence components value.

### A. Consequence of Approximation in LV Network Impedance

The perfect-grounding assumption is equivalent to Kron's reduction of the neutral in a 4-conductor network, whereas the diagonalization step assumes the original 4-conductor network to be balanced. Urquhart and Thomson [7] show that assuming zero off-diagonal sequence components causes 17% voltage error for a 4-core cable of 100 m in the UK even when a balanced current of 50 A is used. Claeys et al. [8] compare 4-wire networks with explicit grounding and the equivalent Kron-reduced networks for distributed generator dispatch optimisation. They show that using the optimisation result from a Kron-reduced network can lead up to 4% phase-to-neutral error when validated against a 4-wire model. Our work [4] found that significant underestimation of voltage violation occurs under unbalanced loading by assuming network impedance to be balanced. Lastly, using correct impedance data is especially important in contexts such as distribution state estimation, as any model error (e.g. impedance error) will get mixed into the measurement residuals, thereby impacting the most likely network state estimate [9].

### B. Observed Accuracy of Carson's Equations

Carson's equations model the earth as a homogeneous semi-definite solid, creating conductor image underneath the ground and deriving impedance fundamentally by waveform propagation of electrical signal [10], [11]. The original equations are further simplified to the *modified* Carson's equations by eliminating image-dependent coordinate variables. The approximation made by the modified equation has an error of less than 1% compared with its original form [7], [10]. Although Carson's equations are at first derived for overhead lines, they also work well for underground cables with error within 1%

compared with finite element analysis at fundamental frequency [12]. It is shown to be insensitive to ground resistivity and cable depth values [12]. There are other methods analyse impedance fundamentally that involves infinite integral term and different approximation has been made. Ref. [13] details the derivation of impedance and compares approximations of the infinite integral terms between the models from Deri, Alvarado, Noda, Pizarro, Dubanton and Carson, and shows that other methods mainly deviate from Carson's for long distribution lines. Supported by this evidence, the authors believe the modified Carson's equations provide an attractive trade-off between accuracy and simplicity (i.e. closed form, algebraic) and is therefore selected as the method to establish impedances in LV networks.

### C. Alternatives to Carson's Equations

Other than Carson's equations, there are a variety of ways to obtain values for the impedance matrices of overhead lines or cables. In finite element analysis (FEA), detailed schematics of cross-sections of cables, the material types and insulation medium involved are required. Boundary conditions for the solution space are needed for truncating the magnetic field [12]. Because conductors and medium are divided into elements (the mesh), a nonuniform structure can be defined and evaluated. Because of its relative complexity, FEA is often used to validate the assumption of models such as Carson's equations, rather than modelling all cables and lines in the network [14]. For data driven approaches, the applicability of the different proposed methods depends on availability of data. Vanin et al. [9] propose the use of generalized state estimation to estimate the line length of network and series impedance matrices. However, it assumes Kron-reduced impedance with limited types of overhead and cable configuration.

### D. Inverse Problems in Power Systems

Inverse problem studies in power systems focus on the recovery of admittance or network topology from sensor data. Recovery of conductor properties from impedance has been unexplored to our knowledge, particularly works considering Carson's equations explicitly. Yuan et. al [15] use graph theory to show that single-phase network admittance can be uniquely recovered when phasor measurement units are present, or when hidden nodes without measurement are connected with at least 3 nodes with measurement. Low in [16] extends the work in [15] to multi-phase network and shows that admittance can be recovered when the network is radial. Similar work has been done in distribution networks, for instance in [17] Liao et. al apply information theory to recover bus connection using hourly active power profile. Deka et al. in [18] determine operational edges in a radial grid using conditional independence tests and voltage measurement.

Well-known challenges of inverse problems include involvement of discrete variables and potential existence of multiple solutions [19]. Discrete variables causes the problem to be combinatorial in nature and nonlinear equations involved in impedance modelling do not guarantee unique recovery.

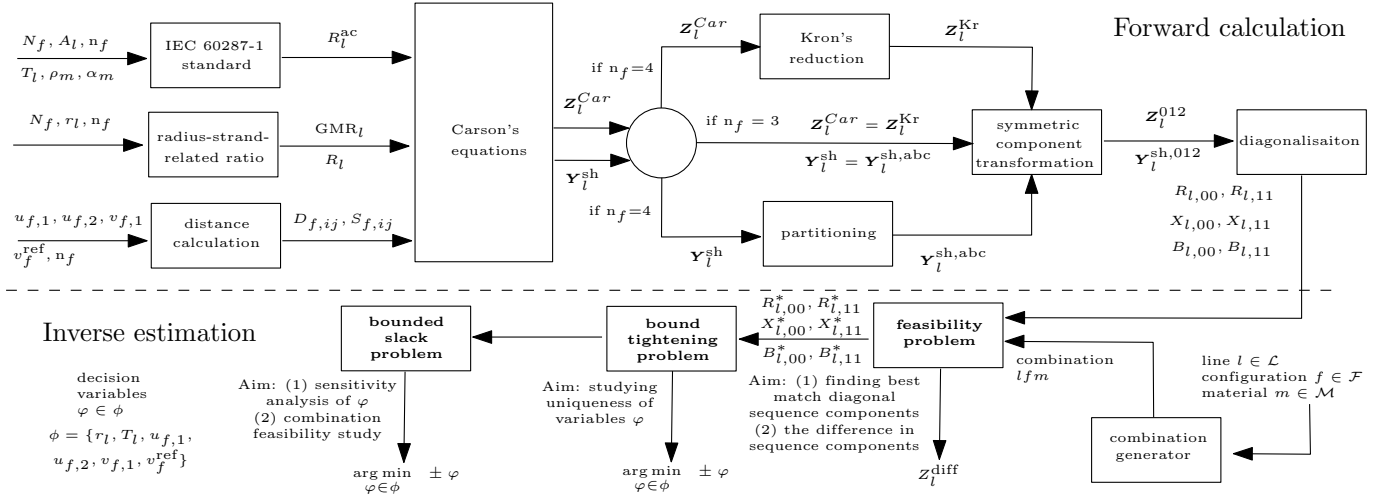


Fig. 2. Computational steps in the forward and inverse Carson's equations solution process.

### E. Discussion

We conclude that there are opportunities in exploiting the structure of Carson's equations to improve the quality of impedance data in existing network datasets. Solving Carson's equations, Kron's reduction and the symmetrical transform as an inverse, maximum likelihood, estimation problem enables modelers to find inconsistencies and inaccuracies in existing network models, and helps establish data improvements.

## III. IMPEDANCE MODELS FOR LOW-VOLTAGE NETWORKS

### A. Derivation of Impedance from First Principles

The mathematical notation used in the paper is summarised in Table I. Index  $i, j \in \mathcal{W} = \{a, b, c, n\}$  is used to refer to different conductors of overhead line or cable, the conductor can be a neutral conductor  $n$  or a phase conductor with phase  $p \in \mathcal{P} = \{a, b, c\}$ . An overhead line or cable has three indices: the line id  $l \in \mathcal{L}$ , the material  $m \in \mathcal{M} = \{\text{Al-1350, Cu}\}$ , and the spatial configuration  $f \in \mathcal{F}$ .

 TABLE I  
SETS AND INDICES.

Subject	Elements in a set
Line	$l \in \mathcal{L}$
Material	$m \in \mathcal{M} = \{\text{Al-1350, Cu}\}$
Configuration	$f \in \mathcal{F}$
Combination	$lfm \in \mathcal{G} \subseteq \mathcal{L} \times \mathcal{F} \times \mathcal{M}$
Conductor	$i, j \in \mathcal{W} = \{a, b, c, n\}$
Phase	$p \in \mathcal{P} = \{a, b, c\}$
Decision variable of interest	$\varphi \in \phi$

The per-length impedance matrix symbols for a 4-conductor overhead line and cable  $l$  with phase and neutral conductors  $abcn$  are defined,

$$\mathbf{Z}_l^{Car} = \mathbf{R}_l^{Car} + j\mathbf{X}_l^{Car} = \begin{pmatrix} Z_{l,aa} & Z_{l,ab} & Z_{l,ac} & Z_{l,an} \\ Z_{l,ba} & Z_{l,bb} & Z_{l,bc} & Z_{l,bn} \\ Z_{l,ca} & Z_{l,cb} & Z_{l,cc} & Z_{l,cn} \\ Z_{l,na} & Z_{l,nb} & Z_{l,nc} & Z_{l,nn} \end{pmatrix} = \begin{pmatrix} \mathbf{Z}_{l,ij} & \mathbf{Z}_{l,in} \\ \mathbf{Z}_{l,nj} & \mathbf{Z}_{l,nn} \end{pmatrix} [\Omega/km]. \quad (1)$$

The per-length self impedance for wire  $i \in \{a, b, c, n\}$  is,

$$Z_{l,ii}^{Car} = R_l^{ac} + 0.049348 + j0.062832 \cdot \left( \ln \frac{1}{c \cdot GMR_l} + 8.0252 \right) [\Omega/km], \quad (2)$$

and the mutual impedance between wires  $i$  and  $j$ , i.e.  $i, j \in \{a, b, c, n\}$ , is,

$$Z_{l,ij}^{Car} = 0.049348 + j0.062832 \cdot \left( \ln \frac{1}{c \cdot D_{f,ij}} + 8.0252 \right) [\Omega/km], \quad (3)$$

where  $R_l^{ac}$  [ $\Omega/km$ ] is the ac resistance of a conductor,  $c$  is a constant of  $3.28084 \cdot 10^{-3}$  [ $\text{mm}^{-1}$ ],  $GMR_l$  [mm] is the geometric mean radius of a conductor and  $D_{f,ij}$  [mm] is the distance between conductors [20]. From (2)-(4), it is observed that  $\mathbf{Z}_l^{Car}$  is guaranteed symmetric in both the real and imaginary parts.

The ac resistance is a function  $h$  of area  $A_l$ , temperature  $T_l$  and material  $m$ . The material determines resistivity  $\rho_m$  and temperature-coefficient  $\alpha_m$ ,

$$R_l^{ac} = h(\rho_m, \alpha_m, T_l, A_l). \quad (4)$$

Kron's reduction of the neutral is performed to transform the network into a reduced  $3 \times 3$  matrix  $\mathbf{Z}_l^{Kr}$  by assuming neutral voltage to be zero,

$$\mathbf{Z}_l^{Kr} = \mathbf{R}_l^{Kr} + j\mathbf{X}_l^{Kr} = \mathbf{Z}_{l,ij} - \frac{1}{Z_{l,nn}} \mathbf{Z}_{l,in} \mathbf{Z}_{l,nj}. \quad (5)$$

The sequence impedance matrix  $\mathbf{Z}_l^{012}$  is now derived from the Kron-reduced matrix,

$$\mathbf{Z}_l^{012} = \mathbf{R}_l^{012} + j\mathbf{X}_l^{012} = \mathbf{A}^{-1} \mathbf{Z}_l^{Kr} \mathbf{A}. \quad (6)$$

The entries in the sequence matrix are,

$$\mathbf{Z}_l^{012} = \begin{pmatrix} Z_{l,00} & Z_{l,01} & Z_{l,02} \\ Z_{l,10} & Z_{l,11} & Z_{l,12} \\ Z_{l,20} & Z_{l,21} & Z_{l,22} \end{pmatrix}. \quad (7)$$

Note that the diagonal entries are called to zero (00), positive (11) and negative sequence (22) impedance, and the positive and negative impedance are equal. Although  $\mathbf{Z}_l^{Car}$  is symmetric, the sequence transformation generally destroys that symmetry, e.g.  $Z_{l,10} \neq Z_{l,01}$ .

The symmetrical component transformation matrix  $\mathbf{A}$  is,

$$\mathbf{A} = \mathbf{A}^{re} + j\mathbf{A}^{im} = \begin{pmatrix} 1 & 1 & 1 \\ 1 & \alpha^2 & \alpha \\ 1 & \alpha & \alpha^2 \end{pmatrix} \\ = \begin{pmatrix} 1 & 1 & 1 \\ 1 & -\frac{1}{2} & -\frac{j\sqrt{3}}{2} \\ 1 & -\frac{1}{2} & \frac{j\sqrt{3}}{2} \end{pmatrix} + j \begin{pmatrix} 0 & 0 & 0 \\ 0 & -\frac{\sqrt{3}}{2} & \frac{1}{2} \\ 0 & \frac{\sqrt{3}}{2} & -\frac{1}{2} \end{pmatrix},$$

with  $\alpha = e^{2\pi/3}$ , and its inverse is,

$$\mathbf{A}^{-1} = \frac{1}{3}\mathbf{A}^{re} + j\frac{-1}{3}\mathbf{A}^{im}.$$

Despite shunt admittance being small to be negligible for overhead lines, underground cables have a higher shunt admittance [21]. Although unfortunately sequence shunt admittance is usually not recorded by utilities, the modelling of sequence shunt admittance is provided in this paper for completeness of modelling. Shunt conductance due to leakage current between conductors and insulation medium is neglected because it is very small compared to shunt susceptance [21].

To derive sequence admittance for shunt, the potential coefficient matrix  $\mathbf{P}_l^{Car}$  of line  $l$  is firstly derived [21],

$$\mathbf{P}_l^{Car} = \begin{pmatrix} P_{l,aa} & P_{l,ab} & P_{l,ac} & P_{l,an} \\ P_{l,ba} & P_{l,bb} & P_{l,bc} & P_{l,bn} \\ P_{l,ca} & P_{l,cb} & P_{l,cc} & P_{l,cn} \\ P_{l,na} & P_{l,nb} & P_{l,nc} & P_{l,nn} \end{pmatrix}. \quad (8)$$

The self and mutual entries are defined,  $i, j \in \{a, b, c, n\}$ ,

$$P_{l,ii} = 17.98742 \cdot \ln \left( \frac{S_{f,ii}}{R_l} \right) [km/uF], \quad (9a)$$

$$P_{l,ij} = 17.98742 \cdot \ln \left( \frac{S_{f,ij}}{D_{f,ij}} \right) [km/uF], \quad (9b)$$

where  $S_{f,ii}$  is the distance [mm] between conductor  $i$  of line  $l$  and its image below ground.  $S_{f,ij}$  [mm] is the distance between actual conductor  $i$  and image of another conductor  $j$ ,  $R_l$  is the radius [mm] of a conductor.

The capacitance matrix  $\mathbf{C}_l^{sh}$  is the matrix inverse of  $\mathbf{P}_l^{Car}$ ,

$$\mathbf{C}_l^{sh} = (\mathbf{P}_l^{Car})^{-1}, \quad (10)$$

and is used to compute the shunt admittance matrix  $\mathbf{Y}_l^{sh}$  at fundamental frequency  $f_l^{fund}$ ,

$$\mathbf{Y}_l^{sh} = j2\pi f_l^{fund} \mathbf{C}_l^{sh}, \quad (11)$$

which also gets partitioned,

$$\mathbf{Y}_l^{sh} = \begin{pmatrix} Y_{l,aa} & Y_{l,ab} & Y_{l,ac} & Y_{l,an} \\ Y_{l,ba} & Y_{l,bb} & Y_{l,bc} & Y_{l,bn} \\ Y_{l,ca} & Y_{l,cb} & Y_{l,cc} & Y_{l,cn} \\ Y_{l,na} & Y_{l,nb} & Y_{l,nc} & Y_{l,nn} \end{pmatrix} \\ = \begin{pmatrix} \mathbf{Y}_l^{sh,abc} & \mathbf{Y}_{l,in}^{sh} \\ \mathbf{Y}_{l,in}^{sh} & Y_{l,nn}^{sh} \end{pmatrix}. \quad (12)$$

Similarly, the sequence admittance matrix  $\mathbf{Y}_l^{sh,012}$  can be obtained by performing symmetric component transformation over the partitioned shunt admittance  $\mathbf{Y}_l^{sh}$  [22],

$$\mathbf{Y}_l^{sh,012} = \mathbf{A}^{-1} \mathbf{Y}_l^{sh,abc} \mathbf{A}. \quad (13)$$

### B. Expressions for $GMR_l$ and $D_{f,ij}$ w.r.t. Coordinates

Carson's equations require values of  $GMR_l$  and  $D_{f,ij}$  to derive the impedance. The  $GMR_l$  of a conductor is related to its radius  $r_l$  by a ratio  $K_f^{gmr}$ . The ratio  $K_f^{gmr}$  depends on the number of strands  $N_f$  and strand geometry [23],

$$GMR_l = K_f^{gmr} \cdot r_l, \quad r_l \& GMR_l \geq 0. \quad (14)$$

We assume all conductors have the same radius  $r_l$  and hence  $GMR_l$ . To compute  $D_{f,ij}$ , Cartesian coordinates is adopted and  $D_{f,ij}$  is defined to be the distance between the center of circular stranded conductors. Although this approach is a simplified alternative to calculate the geometric mean distance (GMD) between strands of conductors, Urquhart and Thomson report that this approach only gives negligible difference compared with GMD and is less subject to rounding error [12]. For a system with  $n_f$  conductors, the x- and y-coordinate of circular-stranded conductors are contained in vectors  $\mathbf{x}_f$  and  $\mathbf{y}_f$  of length  $n_f$ , respectively,

$$\mathbf{x}_f = (x_{f,1} \ \dots \ x_{f,n})^T, \quad \mathbf{y}_f = (y_{f,1} \ \dots \ y_{f,n})^T. \quad (15)$$

The (natural) Euclidean and mirror-image 'distances' are,

$$D_{f,ij} = \sqrt{(x_{f,i} - x_{f,j})^2 + (y_{f,i} - y_{f,j})^2}, \quad (16a)$$

$$S_{f,ij} = \sqrt{(x_{f,i} - x_{f,j})^2 + (y_{f,i} + y_{f,j})^2}. \quad (16b)$$

### C. Likely Geometry for Overhead

For overhead lines, there are many pole geometries, but in this work they are limited to the most common configurations depicted in Fig. 3. For the sake of convenience, free variables  $u_{f,1} \leq u_{f,2} \leq \dots \leq u_{f,n}$  are taken to describe horizontal coordinates in  $\mathbf{x}_f$  and similarly  $v_{f,1} \leq v_{f,2} \leq \dots \leq v_{f,n}$  for vertical coordinates in  $\mathbf{y}_f$ , with all of them being nonnegative.

Next, geometries follow some practical constraints. Firstly, air is assumed to be the only insulation medium so a minimal distance  $D_f^{min}$  between wire applies. Next, the crossarm has a finite length, which is an upper bound for the distance between wires,  $u_f^{max,OH}$ . Lastly, all wires share the same reference distance above ground  $v_f^{ref}$ , which is subject to height limitation,

$$v_f^{ref,min} \leq v_f^{ref} \leq v_f^{ref,max}. \quad (17)$$

1) *Horizontal Plane (4-wire)*: This is the simplest geometry of four wires such that wires are placed apart from the center of the pole by either  $u_{f,1}$  or  $u_{f,2}$ . Neutral wire is assumed to be located furthest from the pole center, e.g.  $(x_4, y_4) = (u_{f,2}, v_f^{ref})$ , and the coordinate vectors are,

$$\mathbf{x}_f = (-u_{f,2} \ -u_{f,1} \ u_{f,1} \ u_{f,2})^T, \quad (18a)$$

$$\mathbf{y}_f = v_f^{ref} \cdot (1 \ 1 \ 1 \ 1)^T. \quad (18b)$$

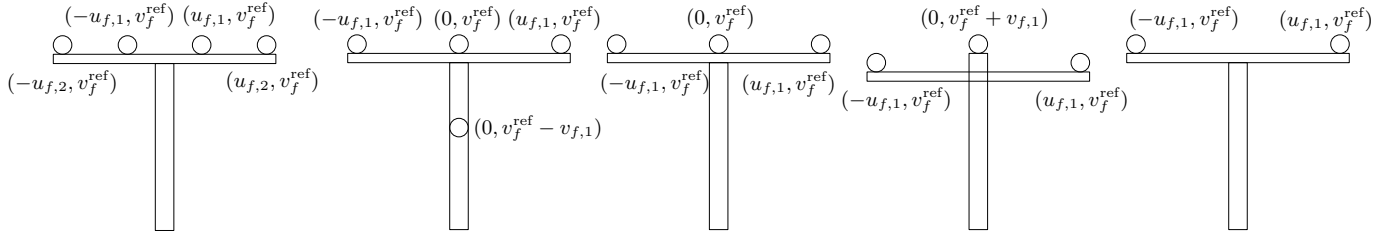


Fig. 3. Overhead line geometries; from left to right: 4-wire horizontal plane, 4-wire neutral-under, 3-wire flat intermediate, 3-wire triangular arrangement and 2-wire horizontal plane.

The minimum distance constraint is defined on the horizontal coordinates. The two outermost wires must be within the half-side crossarm length of  $u_f^{\max,OH}$ , and separated from the two wires near the center of the pole with at least  $D_f^{\min}$ ,

$$u_f^{\max,OH} \geq u_{f,2} \geq u_{f,1} + D_f^{\min}. \quad (19)$$

Next, the two wires near the center of the pole must be separated from each other by at least  $D_f^{\min}$ ,

$$u_{f,1} \geq D_f^{\min}/2. \quad (20)$$

2) *Neutral-under (4-wire)*: This geometry has 3 phase wires on the top and a neutral wire under the phase wire

$$\mathbf{x}_f = (-u_{f,1} \ 0 \ 0 \ u_{f,1})^T, \quad (21a)$$

$$\mathbf{y}_f = (v_f^{\text{ref}} \ v_f^{\text{ref}} \ v_f^{\text{ref}} - v_{f,1} \ v_f^{\text{ref}})^T. \quad (21b)$$

Distances are upper bounded by crossarm length and maintain minimal distance of  $D_f^{\min}$  from each other,

$$u_f^{\max,OH} \geq u_{f,1} \geq D_f^{\min}. \quad (22)$$

The neutral wire is above ground and below the center phase wire by at least  $D_f^{\min}$ ,

$$v_f^{\text{ref}} \geq v_{f,1} \geq D_f^{\min}. \quad (23)$$

3) *Horizontal Plane (3-wire)*: One wire is placed at the top center of the pole and the remaining two away from the center with distance  $u_{f,1}$ ,

$$\mathbf{x}_f = (-u_{f,1} \ 0 \ u_{f,1})^T, \quad \mathbf{y}_f = v_f^{\text{ref}} (1 \ 1 \ 1)^T. \quad (24)$$

In this configuration, distance constraint (22) also applies.

4) *Triangular Arrangement (3-wire)*: In this geometry 3 wires form an isosceles triangle such that one wire is placed at the center of the pole above the crossarm, and two wires are placed  $u_{f,1}$  away from the center of pole.

$$\mathbf{x}_f = (-u_{f,1} \ 0 \ u_{f,1})^T, \quad \mathbf{y}_f = (v_f^{\text{ref}} \ v_f^{\text{ref}} + v_{f,1} \ v_f^{\text{ref}})^T. \quad (25)$$

$\tan(\theta)$  is the ratio between  $v_{f,1}$  and  $v_{f,1}$ ,

$$v_{f,1} = u_{f,1} \cdot \tan(\theta). \quad (26)$$

The two wires on the crossarm are separated by at least  $D_f^{\min}$  and each wire on the crossarm should be at least  $D_f^{\min}$  away from the wire on the top of the pole. Finally, the lower bound on  $u_{f,1}$  needs to consider both conditions,

$$u_f^{\max,OH} \geq u_{f,1} \geq \max\{D_f^{\min}/2, D_f^{\min} \cdot \cos \theta\}. \quad (27)$$

5) *Horizontal Plane (2-wire)*: This is a common arrangement for single-phase connection. Two lines are equally separated from the middle of the pole,

$$\mathbf{x}_f = (-u_{f,1} \ u_{f,1})^T, \quad \mathbf{y}_f = v_f^{\text{ref}} (1 \ 1)^T. \quad (28)$$

Similarly, distance bound apply for  $u_{f,1}$ ,

$$u_f^{\max,OH} \geq u_{f,1} \geq D_f^{\min}/2. \quad (29)$$

#### D. Likely Geometry for Low-voltage Aerial Bundle Cable and Underground Cable

Common geometries of 4-core, 3-core and 2-core cables are shown in Fig. 4. It is assumed that radius  $R_l^{\text{nom}}$  of all cores are the same and all cores are closely packed symmetrically in a cable. Common cables type in low-voltage application are circular stranded with each core insulated with thickness  $t^{\text{nom}}$ . Because all cores in a cable are closely-packed, it is convenient to express the Cartesian coordinates in terms of core radius  $R_l^{\text{nom}}$ . To begin with,  $R_l^{\text{nom}}$  is derived from the strand radius  $r_l$  and the core insulation thickness  $t^{\text{nom}}$ ,

$$R_l^{\text{nom}} = R_l + t^{\text{nom}}, \quad R_l = K_f^r \cdot r_l. \quad (30)$$

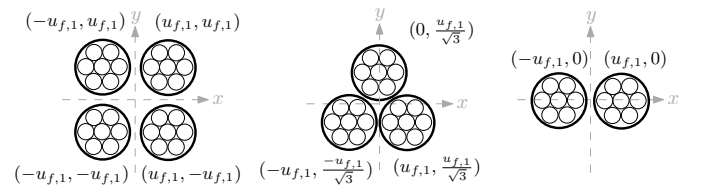


Fig. 4. Cable geometry normalised in  $R_l^{\text{nom}}$ : from left to right are 4-core square, 3-core equilateral triangle and two-core closely-packed horizontal. Reference height of cables are not shown for simplicity of illustration.

The packing coefficient  $K^r$  is the coefficient relating radius of strand and radius of core excluding the core insulation thickness. The term  $K_f^r \cdot r_l$  is the minimal radius of core required to pack all strands without insulation. A lower bound on  $R_l^{\text{nom}}$  is derived by assuming no insulation thickness:

$$R_l^{\text{nom}} \geq K_f^r \cdot r_l. \quad (31)$$

To be consistent with overhead notation for distance,  $R_l^{\text{nom}}$  is set to equal to  $u_{f,1}$ ,

$$u_{f,1} = R_l^{\text{nom}}. \quad (32)$$

1) *4-conductor*: This is the geometry for both 4-core circular- and sector-stranded cable<sup>1</sup>,

$$\mathbf{x}_f = u_{f,1} \cdot (1 \quad -1 \quad -1 \quad 1)^T, \quad (33a)$$

$$\mathbf{y}_f = u_{f,1} \cdot (1 \quad 1 \quad -1 \quad -1)^T + v_f^{\text{ref}}. \quad (33b)$$

Reference cable height  $v_f^{\text{ref}}$  is added to the local y-coordinate.

2) *3-conductor*: The 3 cores form an equilateral triangle,

$$\mathbf{x}_f = u_{f,1} \cdot (-1 \quad 0 \quad 1)^T, \quad (34a)$$

$$\mathbf{y}_f = u_{f,1}/\sqrt{3} \cdot (-1 \quad 2 \quad -1)^T + v_f^{\text{ref}}. \quad (34b)$$

3) *2-conductor*: The 2 cores are adjacent,

$$\mathbf{x}_f = u_{f,1} \cdot (-1 \quad 1)^T, \quad (35a)$$

$$\mathbf{y}_f = v_f^{\text{ref}} \cdot (1 \quad 1)^T. \quad (35b)$$

### E. Electrical Characteristic Modelling of Material

The IEC 60287-1-1 standard is adopted for deriving the ac resistance and details of function  $h$  in (4) is now expanded. For conductors with single material  $m$ , e.g. Aluminium or Copper, the ac resistance  $R_l^{\text{ac}}$  is derived as follows. Firstly, the cross sectional area  $A_l$  of circular-stranded conductor is the sum of cross sectional area of  $N$  strands,

$$A_l = N_f \pi r_l^2. \quad (36)$$

Then, the dc resistance of conductor  $R_l^{\text{dc}}$  at 20 °C is obtained through dividing the material resistivity  $\rho_m$  at 20 °C by the cross sectional area  $A_l$ . Next,  $R_l^{\text{dc}}$  at the expected temperature  $T_l$  is derived using the material temperature coefficient  $\alpha_m$ ,

$$R_l^{\text{dc}} = \frac{\rho_m}{A_l} (1 + \alpha_m (T_l - 20^\circ\text{C})). \quad (37)$$

We assume all conductors share the same temperature  $T_l$ . Now, ac resistance  $R_l^{\text{ac}}$  is calculated by considering increase in resistance due to skin effect  $C_l^s$  and proximity effect  $C_l^p$ .

$$R_l^{\text{ac}} = (1 + C_l^s)(1 + C_l^p)R_l^{\text{dc}}. \quad (38)$$

The radius, area and temperature range of conductors are bounded over practical values for the inverse problem,

$$r_l^{\min} \leq r_l \leq r_l^{\max}, \quad (39a)$$

$$A_l^{\min} \leq A_l \leq A_l^{\max}, \quad (39b)$$

$$T_l^{\min} \leq T_l \leq T_l^{\max}. \quad (39c)$$

## IV. INVERSE PROBLEM AS AN OPTIMIZATION PROBLEM

We assume utilities only provide reference sequence components  $R_{l,00}^{\text{ref}}, R_{l,11}^{\text{ref}}, X_{l,00}^{\text{ref}}, X_{l,11}^{\text{ref}}, B_{l,00}^{\text{ref}}, B_{l,11}^{\text{ref}}$ , without information of discrete properties material  $m$  and configuration  $f$  (which contains discrete information of number of conductor  $n$ , number of strands  $N$  and type of geometry), the discrete properties are combined to form combination  $lfm \in \mathcal{G} \subseteq$

<sup>1</sup>In the forward calculation, sector-stranded geometry follows Fig. 9b of [23]  $\text{GMR}_l$  and  $D_{f,ij}$  are calculated using (10) and (14) of [20], which results in slightly rectangular geometry. In inverse estimation, we assume square geometry for simplification of analysis. Eq. (30) does not hold for sector-stranded cable. But Eq. (31) holds and is validated by setting  $t^{\text{nom}}=0$  and iterating  $A_l$  from 185-300mm<sup>2</sup> in forward calculation.

$\mathcal{L} \times \mathcal{F} \times \mathcal{M}$ , which is optimised to match the reference sequence components.

As illustrated in Fig. 2, the inverse problem is split into three sequential steps, each cast as optimisation problems, namely 1) the feasibility problem, 2) the bound tightening problem and 3) the bounded slack problem. In the feasibility problem, a combination  $lfm$  is optimised to return the sequence components closest to the reference sequence components given. The closer it is, the more likely a combination is a correct estimation. In the bound tightening problem, the range of decision variables returned from from feasibility problem is studied. This provides numerical evidence of the uniqueness of the solution to the feasibility problem. Lastly, in the bounded slack problem, sensitivity of decision variables over reference sequence components will be analysed. It studies the range of decision variables when there is slack in the reference sequence components. Also, it investigates how much slack is required for an incorrect combination to be a feasible solution to match the reference sequence components. It provides an understanding how resilient decision variables are when potential error are introduced in sequence component data, such as using wrong fundamental frequency (50 or 60 Hz) or different variants of Carson's equations.

### A. Feasibility Problem

The distance of diagonal impedance and susceptance sequence components  $Z_l^{\text{diff}}$  between a combination  $lfm$  and the reference components is minimised. The error terms within the absolute operators in (40) represent  $\ell_1$  norms, which induce sparsity in the error terms, to minimise error propagation across different sequence component values. Next, it is normalised by the corresponding reference sequence component value and divided by 6, i.e.,

$$Z_l^{\text{diff}} = \left( \frac{1}{B_{l,00}^{\text{ref}}} \underbrace{|B_{l,00} - B_{l,00}^{\text{ref}}|}_{B_{l,00}^{\text{aux}}} + \frac{1}{B_{l,11}^{\text{ref}}} \underbrace{|B_{l,11} - B_{l,11}^{\text{ref}}|}_{B_{l,11}^{\text{aux}}} + \frac{1}{R_{l,00}^{\text{ref}}} \underbrace{|R_{l,00} - R_{l,00}^{\text{ref}}|}_{R_{l,00}^{\text{aux}}} + \frac{1}{R_{l,11}^{\text{ref}}} \underbrace{|R_{l,11} - R_{l,11}^{\text{ref}}|}_{R_{l,11}^{\text{aux}}} + \frac{1}{X_{l,00}^{\text{ref}}} \underbrace{|X_{l,00} - X_{l,00}^{\text{ref}}|}_{X_{l,00}^{\text{aux}}} + \frac{1}{X_{l,11}^{\text{ref}}} \underbrace{|X_{l,11} - X_{l,11}^{\text{ref}}|}_{X_{l,11}^{\text{aux}}} \right) / 6. \quad (40)$$

In case of missing shunt susceptance data, the corresponding terms are dropped from (40), and the division by 6 is replaced with division by 4 (now labelled  $Z_l^{\text{diff,series}}$ ).

$$\begin{aligned} & \min && Z_l^{\text{diff}}, && (41) \\ & \text{var. } && \mathbf{x}_f, \mathbf{y}_f, r_l, D_{f,ij}, S_{f,ij}, T_l, R_l^{\text{dc}}, R_l^{\text{ac}}, A_l, R_l, \\ & && \text{GMR}_l, \mathbf{R}_l^{\text{Car}}, \mathbf{X}_l^{\text{Car}}, \mathbf{R}_l^{\text{Kr}}, \mathbf{X}_l^{\text{Kr}}, \mathbf{R}_l^{012}, \mathbf{X}_l^{012}, \\ & \text{s.t.} && (1) \text{ to } (40). \end{aligned}$$

The optimal values of  $R_{l,00}, X_{l,00}, R_{l,11}, X_{l,11}, B_{l,00}, B_{l,11}$ , as denoted by  $R_{l,00}^*, R_{l,11}^*, X_{l,00}^*, X_{l,11}^*, B_{l,00}^*, B_{l,11}^*$  respectively, will be passed to bound-tightening problem.

### B. Bound Tightening Problem

The range of decision variables is investigated by evaluating their minimal and maximal values. Each decision variable  $\varphi \in \phi = \{r_l, T_l, u_{f,1}, u_{f,2}, v_{f,1}\}$  is iterated individually. A negative sign in (42) effectively indicates maximisation. Note that the optimal sequence components values with asterisk obtained from the previous feasibility problem will be used here as shown in (42b) - (42d).

$$\min_{\varphi \in \phi} \quad \pm \varphi, \quad (42a)$$

$$\text{var. } \mathbf{x}_f, \mathbf{y}_f, r_l, D_{f,ij}, S_{f,ij}, T_l, R_l^{dc}, R_l^{ac}, A_l, R_l, \\ \text{GMR}_l, \mathbf{R}_l^{Car}, \mathbf{X}_l^{Car}, \mathbf{R}_l^{Kr}, \mathbf{X}_l^{Kr}, \mathbf{R}_l^{012}, \mathbf{X}_l^{012},$$

$$\text{s.t.} \quad (1) \text{ to } (39c),$$

$$R_{l,00} = R_{l,00}^*, R_{l,11} = R_{l,11}^*, \quad (42b)$$

$$X_{l,00} = X_{l,00}^*, X_{l,11} = X_{l,11}^*, \quad (42c)$$

$$B_{l,00} = B_{l,00}^*, B_{l,11} = B_{l,11}^*. \quad (42d)$$

Note that only diagonal entries are fixed while the off-diagonal entries in  $\mathbf{R}_l^{012}, \mathbf{X}_l^{012}$  remain free.

### C. Bounded Slack Problem

Sensitivity analysis of decision variables  $\varphi$  in  $\phi$  over reference sequence components are conducted by introducing slack  $\beta$  to the reference sequence components as shown in (43b) to (43g).

$$\min_{\varphi \in \phi} \quad \pm \varphi, \quad (43a)$$

$$\text{var. } \mathbf{x}_f, \mathbf{y}_f, r_l, D_{f,ij}, S_{f,ij}, T_l, R_l^{dc}, R_l^{ac}, A_l, R_l, \\ \text{GMR}_l, \mathbf{R}_l^{Car}, \mathbf{X}_l^{Car}, \mathbf{R}_l^{Kr}, \mathbf{X}_l^{Kr}, \mathbf{R}_l^{012}, \mathbf{X}_l^{012},$$

$$\text{s.t.} \quad (1) \text{ to } (39c),$$

$$(1 - \beta)R_{l,00}^{\text{ref}} \geq R_{l,00} \geq (1 + \beta)R_{l,00}^{\text{ref}}, \quad (43b)$$

$$(1 - \beta)R_{l,11}^{\text{ref}} \geq R_{l,11} \geq (1 + \beta)R_{l,11}^{\text{ref}}, \quad (43c)$$

$$(1 - \beta)X_{l,00}^{\text{ref}} \geq X_{l,00} \geq (1 + \beta)X_{l,00}^{\text{ref}}, \quad (43d)$$

$$(1 - \beta)X_{l,11}^{\text{ref}} \geq X_{l,11} \geq (1 + \beta)X_{l,11}^{\text{ref}}, \quad (43e)$$

$$(1 - \beta)B_{l,00}^{\text{ref}} \geq B_{l,00} \geq (1 + \beta)B_{l,00}^{\text{ref}}, \quad (43f)$$

$$(1 - \beta)B_{l,11}^{\text{ref}} \geq B_{l,11} \geq (1 + \beta)B_{l,11}^{\text{ref}}. \quad (43g)$$

Slack  $\beta$  is introduced in the reference sequence components to study when incorrect inverse estimation becomes feasible.

### D. Reformulation as Differentiable Equations in the Reals

Optimization modeling toolboxes (typically) do not support complex numbers, so for implementation purposes equations are re-stated in real variables. Next, the square root and absolute value functions are non-differentiable whereas division operation requires addition of nonlinear constraint, so they are reformulated as quadratic equations.

Firstly, the absolute value terms is reformulated by introducing auxiliary variables to represent the value of the absolute value of the difference, i.e.,

$$\min |a - b|, \text{ s.t. } a, b \in \mathbb{R},$$

$$\iff \min c, \text{ s.t. } c \geq a - b, c \geq b - a \implies c = |a - b|.$$

Next, Kron's reduction (5) and the symmetrical component transform (6) are equivalently restated in the reals as quadratic and linear equations respectively.

The square-root is removed by squaring both side of (16) and (17),

$$(D_{f,ij})^2 = (x_{f,i} - x_{f,j})^2 + (y_{f,i} - y_{f,j})^2, D_{f,ij} \geq 0, (44)$$

$$(S_{f,ij})^2 = (x_{f,i} - x_{f,j})^2 + (y_{f,i} + y_{f,j})^2, S_{f,ij} \geq 0. (45)$$

Lastly, division operation in (37) is removed by rearrangement of variables,

$$R_l^{dc} \cdot A_l = \rho_m(1 + \alpha_m(T_l - 20)), \quad R_l^{dc} \geq 0. \quad (46)$$

## V. TEST CASE AND VALIDATION

### A. Scenario and Computation Set-up

The inverse problem is set up in Julia (v1.8.3) with optimisation modelling language JuMP and solver Ipopt. Ipopt in combination with JuMP's automatic differentiation allows the formulation of optimisation problems with quadratic and transcendental constraints. The computation is performed on an Intel(R) Core(TM) i7-11700 @ 2.50 GHz with 32 GB RAM. The forward calculation result is validated against OpenDSS with results matched up to 4 decimal places in  $[\Omega/\text{km}]$ .

The test case for validation as summarised in Table II considers overhead line and cables commonly adopted in LV network in Eastern Australia [24], [25], which the authors of this paper have knowledge on.

Two-wire overhead lines and two-core cables are excluded because using sequence coordinates to represent their impedance is misleading. Transformer impedance are out-of-scope. Next, skin and proximity effect are excluded by setting  $C_l^s = C_l^p = 0$  to avoid the associated non-linear equations as per IEC 60287-1-1 standard [26]. This is a mild assumption based on the study from Urquhart and Thomson that for a large 300 mm<sup>2</sup> cable, the combined skin and proximity effect together account for only 2% in ac resistance [12]. Next, shunt susceptance is excluded because it is usually not provided by utilities. Therefore, metric  $Z_l^{\text{diff,series}}$  instead of  $Z_l^{\text{diff}}$  is used in the feasibility problem. Lastly, it is assumed that utility can provide all diagonal sequence components  $R_{l,00}^{\text{ref}}, R_{l,11}^{\text{ref}}, X_{l,00}^{\text{ref}}, X_{l,11}^{\text{ref}}$  and know whether they belong to overhead line or cable.

### B. Data on Overhead Lines and Cables

From Table II, overhead lines in Australia are typically 7-strand Aluminium wire. Two 4-wire geometries and three 3-wire geometries, as summarised in Table III, are adopted in Australia. Therefore, overhead lines only differ in configuration  $f$ . For cables, it has different number of cores (3 / 4), number of strands (7 / 19 / 48) and material (Al-1350 / Cu), therefore cables differ in both configuration  $f$  ( which contains  $n_f$  and  $N_f$ ) and material  $m$ .

Samples of overhead lines and cables are created to generate a variety of sequence impedance components in forward calculation, through iteration of area with step 5 mm<sup>2</sup>, temperature with step 5 °C, material in Table V and configuration in Table IV over practical range as summarised in Table VI. In inverse estimation, assuming there is no knowledge of

TABLE II  
COMMON OVERHEAD LINE AND CABLE FOR LV NETWORK IN  
QUEENSLAND AUSTRALIA [24] [25].

$l \in \mathcal{L}$	$ \mathcal{W} $	$A_l$ [mm <sup>2</sup> ]	$r_l$ [mm]	$N_f$	$m$	$t^{\text{nom}}$ [mm]
OH Libra	3 or 4	49.48	1.5	7	Al-1350	N/A
OH Mars	3 or 4	77.31	1.875	7	Al-1350	N/A
OH Moon	3 or 4	124.04	2.375	7	Al-1350	N/A
LVABC4x95	4	94.75	1.26	19	Al-1350	1.7
LVABC4x50	4	48.17	1.48	7	Al-1350	1.5
LVABC4x25	4	26.61	1.1	7	Al-1350	1.3
LVABC3x25	3	26.61	1.1	7	Al-1350	1.3
UGC16x4Cu	4	15.89	0.85	7	Cu	1
UGC50x4Cu	4	48.17	1.48	7	Cu	1.5
UGC240x4Al	4	239.40	1.26	48	Al-1350	1.7

TABLE III  
PARAMETERS FOR FORWARD CALCULATION [24] [27]. FOR OH  
NEUTRAL-UNDER,  $u_{f,1}$  AND  $v_{f,1}$  ARE THE AVERAGED VALUES OF FIG. 5  
OF [28] AND ITS MIRROR IMAGE. FOR CABLE,  $t^{\text{nom}}=1.5$  MM AND  
 $v_f^{\text{REF}}=-1$  M ARE ASSUMED [25].

$f^{l,\text{OH}} \in \mathcal{F}^{l,\text{OH}}$	$ \mathcal{W} $	$u_{f,1}$ [mm]	$u_{f,2}$ [mm]	$v_{f,1}$ [mm]	$v_f^{\text{ref}}$ [mm]
OH horizontal plane	4	450	1100	N/A	9150
OH neutral-under	4	1118	N/A	1575	9150
OH horizontal plane	3	1100	N/A	N/A	9150
OH triangular ( $\theta=21.67^\circ$ )	3	1100	N/A	437	9150
OH triangular ( $\theta=49.27^\circ$ )	3	508	N/A	590	9150

which configuration are the sequence components generated from (and no knowledge of material if it is a cable) but knowing whether it is a cable or overhead line, combinations are therefore formed by iterating the samples by configuration (and material if it is a cable). Note that forward calculations using too small or large areas result in radius smaller than  $r_l^{\text{min}}$  or larger than  $r_l^{\text{max}}$  shown in Table VII are removed to prevent violation of radius bound in (39a).

### C. Feasibility Problem Result

For overhead lines, Fig. 5 shows that when the number of wires is incorrectly estimated in a combination, values

TABLE IV  
CONFIGURATION PARAMETERS, ( $v_f^{\text{REF,MIN}}, v_f^{\text{REF,MAX}}$ ) IN [m] FOR OH AND  
CABLE ARE (5.8,21.5) AND (-6,0.6) RESP. [24] [25].

$f \in \mathcal{F}^{\text{OH}}$	$ \mathcal{W} $	$N_f$	$K_f^{\text{gmr}}$	$K_f^r$	$D_f^{\text{min}}$ [mm]	$u_f^{\text{max,OH}}$ [mm]
OH hori. plane	3	7	2.18	3	380	1500
OH tri. ( $\theta=21.67^\circ$ )	3	7	2.18	3	380	1500
OH tri. ( $\theta=49.27^\circ$ )	3	7	2.18	3	380	1500
OH hori. plane	4	7	2.18	3	380	1500
OH neutral-under	4	7	2.18	3	380	1500
$f \in \mathcal{F}^{\text{cable}}$	$ \mathcal{W} $	$N_f$	$K_f^{\text{gmr}}$	$K_f^r$	$u_f^{\text{min,cable}}$ [mm]	$u_f^{\text{max,cable}}$ [mm]
Cable 3w7N circ.	3	7	2.18	3	2.55	27.5
Cable 3w19N circ.	3	19	3.79	5	2.55	27.5
Cable 4w7N circ.	4	7	2.18	3	2.55	27.5
Cable 4w19N circ.	4	19	3.79	5	2.55	27.5
Cable 4w48N sect.	4	48	6.41	6.89	2.55	27.5

TABLE V  
MATERIAL PARAMETERS.

$m \in \mathcal{M}$	$\rho_m$ [10 <sup>-9</sup> Ω · m]	$\alpha_m$ [1/°C]	Standard
Al-1350	28.3	0.00403	AS3607-1989 [29]
Cu	17.77	0.00381	AS1746-1991 [30]

TABLE VI  
BOUND OF ITERATION, TOP HALF FOR OVERHEAD LINE AND BOTTOM  
HALF FOR CABLE.

Var.	Range/Set	Unit	Justification
$A_l$	[15,240]	mm <sup>2</sup>	Min. and max. area in Table II.
$T_l$	[20,75]	°C	Dc resistance temp. and layout temp. [24]
$m$	{Al-1350}	N/A	Assumed material for OH line.
$A_l$	[15,240]	mm <sup>2</sup>	$f^{\text{cable}} \in \mathcal{F}^{\text{cable}}$ excepts Cable 4w48N sect.
$A_l$	[185,300]	mm <sup>2</sup>	For Cable 4w48N sect. 90° sector area of $N_f=37$ and 61 [31]
$T_l$	[20,90]	°C	Cable max. operation temp. is 90°C [25].
$m$	$\mathcal{M}$	N/A	Both Al and Cu are common for cables.

of  $Z_l^{\text{diff,series}}$  range from 0.1 to 0.2. However, a close-to-zero  $Z_l^{\text{diff,series}}$  is observed when it is correctly estimated. This suggests that mismatch of number of wires causes impedance highly deviated from the given sequence impedance.

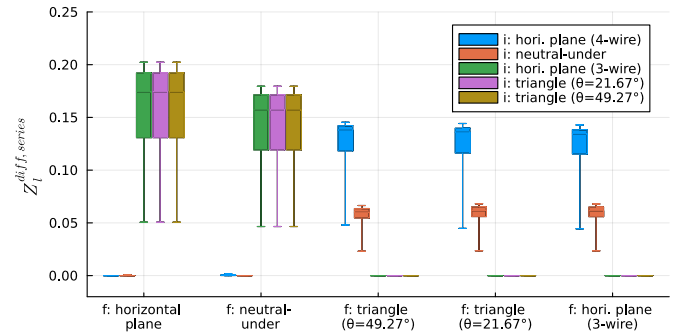


Fig. 5.  $Z_l^{\text{diff,series}}$  for overhead lines with different forward (f:) calculation and inverse (i:) estimation.

For cables, the match and mismatch of three discrete properties  $m$ ,  $N_f$  and  $n_f$  yield  $2^3=8$  combinations. Fig. 6 shows that highest  $Z_l^{\text{diff,series}}$  occurs when mismatch of number of cores occurs. A higher  $Z_l^{\text{diff,series}}$  is seen for mismatch of  $N_f$  than

TABLE VII  
BOUND FOR OPTIMISATION VARIABLES.

Parameter	Value	Justification
$D_f^{\text{min}}$	380 mm	Ausgrid standard [32]
$u_f^{\text{max,OH}}$	1500 mm	Largest crossarm from Energy QLD [24]
$u_f^{\text{min,cable}}$	2.55 mm	UGC16x4Cu core radius w/o $t^{\text{nom}}$ [33]
$u_f^{\text{max,cable}}$	27.7 mm	UGC240x4Al core radius with $t^{\text{nom}}$ [31]
$T_l^{\text{min}}$	0 °C	Arbitrary for simulation purpose
$T_l^{\text{max}}$	105 °C	Emergency operation temp. for cable [25]
$r_l^{\text{min}}$	0.85 mm	Minimum $r_l$ in Table II
$r_l^{\text{max}}$	2.375 mm	Maximum $r_l$ in Table II
$A_l^{\text{min}}, A_l^{\text{max}}$	15,240 mm <sup>2</sup>	Min. and max. area in Table II
$A_l^{\text{min}}, A_l^{\text{max}}$	185,300 mm <sup>2</sup>	Sector area of $N_f=37$ & $N_f=61$ [31]



$m$ . The reason is that practical bounds of radius and area as per (39a) and (39b) limit the minimisation of  $Z_l^{\text{diff,series}}$ . Also, cable of larger area results in larger  $Z_l^{\text{diff,series}}$  when mismatch of  $N_f$  happens.

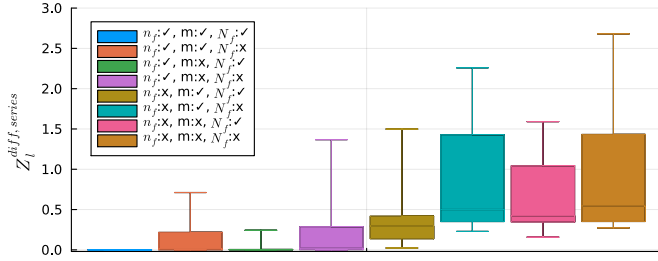


Fig. 6.  $Z_l^{\text{diff,series}}$  for cables with match and mismatch of combination of different discrete properties, as denoted by  $\checkmark$  and  $\times$  respectively.

#### D. Bound Tightening Problem Result

In the bound-tightening problem, (local) uniqueness over decision variables  $\phi = \{r_l, T_l, u_{f,1}, u_{f,2}, v_{f,1}\}$  is studied. To prevent over-constraining, only some feasible solution  $R_{l,00}^*, R_{l,11}^*, X_{l,00}^*, X_{l,11}^*$  are used by the bound-tightening problem, as denoted by  $\checkmark$  in Table VIII. All decision variables  $\varphi \in \phi$  are locally unique as validated by  $\arg \min \varphi = \arg \max \varphi$  for all combinations  $lfm$  up to a tolerance of 1.44 °C for  $T_l$ , 0.0027 mm for  $r_l$ , 0.014 mm for geometry variables  $u_{f,1}, u_{f,2}, v_{f,1}$ .

TABLE VIII

DOF FOR DIFFERENT CASES. TEMPERATURE AND RADIUS  $r_l$  TOGETHER CONSTITUTES 2 DEGREE-OF-FREEDOM (DOF). NUMBER OF GEOMETRY DOF IN  $\{u_{f,1}, u_{f,2}, v_{f,1}\}$  DEPENDS ON CASE.

$ \mathcal{W} $	Type	$T_l$ & $r_l$ DOF	Geo. DOF	Sum DOF	$R_{l,00}^*$	$R_{l,11}^*$	$X_{l,00}^*$	$X_{l,11}^*$
3	OH	2	1	3		$\checkmark$	$\checkmark$	$\checkmark$
3	Cable	2	1	3		$\checkmark$	$\checkmark$	$\checkmark$
4	OH	2	2	4	$\checkmark$	$\checkmark$	$\checkmark$	$\checkmark$
4	Cable	2	1	3	$\checkmark$	$\checkmark$	$\checkmark$	$\checkmark$

#### E. Bounded Slack Problem Result

For overhead line, the number of wires in an overhead line can be reliably distinguished. Fig. 7 shows the feasibility percentage over different inverse configuration when the forward geometry is a 3-wire triangular arrangement with  $\theta=21.67^\circ$ . Inverse geometry of 4 wires are infeasible unless large amount of slack is applied, which suggests that mismatch of number of wires is not likely to happen. Nevertheless, other 3-wire inverse geometries are always feasible regardless of amount of slack because off-diagonal symmetric components which contains unbalance information are missing.

In order to distinguish geometries with the same number of wires, decision variables for all 3-wire geometries are now investigated. Fig. 8 shows the range of  $u_{f,1}$  under different slack for all 3-wire forward geometries. All boxes in the box-plot have a large range of  $u_{f,1}$  even under small slack,

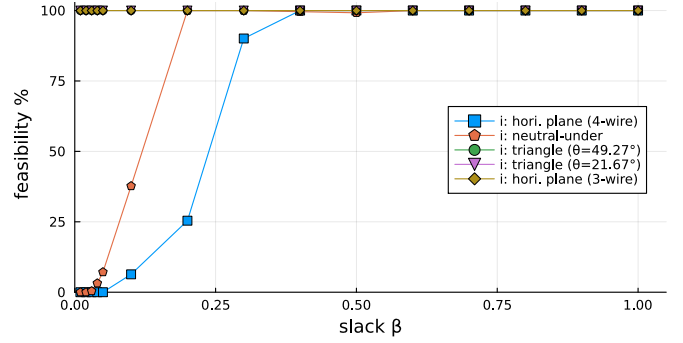


Fig. 7. Feasibility percentage for different configuration when forward geometry is triangle ( $\theta=21.67^\circ$ ).

which suggests that geometry variables are highly sensitive to sequence values. Next, overlapping of  $u_{f,1}$  happens for forward geometry of 3-wire horizontal plane and triangle ( $\theta=21.67^\circ$ ) at all slack but not triangle ( $\theta=49.27^\circ$ ) up to 2% slack. This suggests that the 3-wire horizontal plane and triangle ( $\theta=21.67^\circ$ ) cannot be reliably distinguished but triangle ( $\theta=49.27^\circ$ ) can be distinguished up to 2% slack. By referring to the value of  $u_{f,1}$  for forward calculation in Table III, one can see that  $u_{f,1}$  of triangle ( $\theta=49.27^\circ$ ) is 508 mm, which is highly deviated from  $u_{f,1}=1100$  mm for the other two 3-wire geometries. This suggests that geometries with the same number of wires can only be distinguished reliably if small error is assumed in the the given sequence components and large geometry variable difference exists between construction code of different geometries.

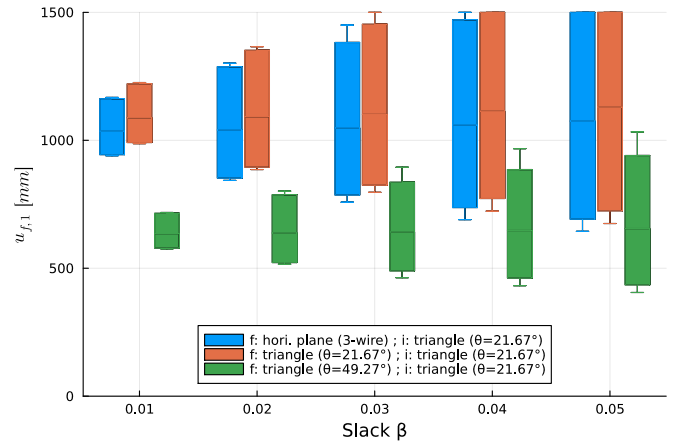


Fig. 8. Range of  $u_{f,1}$  for triangle ( $\theta=21.67^\circ$ ) being the inverse geometry. Variable  $u_{f,1}$  has an upper bound of  $u_f^{\text{max,OH}}=1500$  mm.

For cable, Fig. 9 shows the overall feasibility percentage for different combinations of match or mismatch of discrete properties. It shows mismatch of number of core makes a combination to become infeasible unless high slack is applied. Mismatch of number of strands is more likely to cause a combination to be infeasible than mismatch of material.

## VI. CONCLUSIONS

This paper formulates the recovery of low-voltage network data as an inverse problem from first principles - i.e. Car-

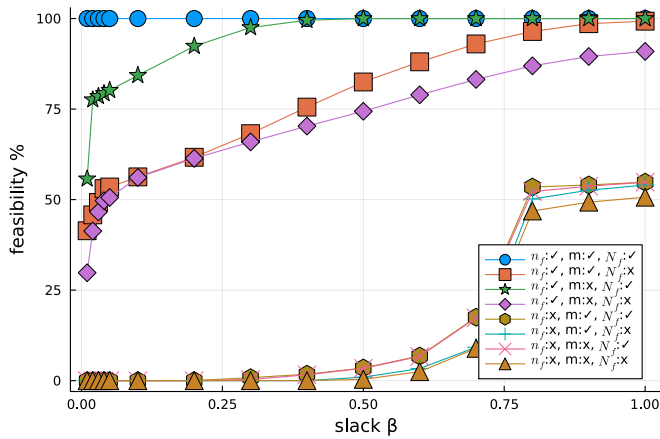


Fig. 9. Match and mismatch of combination of discrete properties against forward calculation are denoted by ✓ and X respectively.

son's equations - determining the best fit w.r.t. the physics for both overhead lines and cables. The inverse problem methodology is composed of three steps, each optimisation problems. For the feasibility problem, an algorithm is proposed which allows combinations of different discrete properties to best match the given sequence components. For the bound-tightening problem, evidence is presented suggesting that the inverse solution is locally unique even when temperature is not given. The bounded-slack problem quantifies the risk of incorrect estimation. For both overhead line and cable, we show that the number of conductors can be reliably recovered. For overhead line, geometry variables are highly sensitive to sequence impedance values, and geometry types can be reliably recovered when small slack is assumed in the given sequence components. For larger cable, we show that mismatch of number of strands happens less often than mismatch of material due to the practical bounds of radius and area. Exploiting the structure of Carson's equations when learning line impedance matrices from smart meter data is a direction of future work.

## REFERENCES

- [1] E. Beckstedde and L. Meeus, "From "fit and forget" to "flex or regret" in distribution grids," *IEEE Power Energy Mag.*, vol. 21, no. 4, pp. 45–52, Jul. 2023.
- [2] Geth *et al.*, "National Low-Voltage Feeder Taxonomy Study," CSIRO, Newcastle, Tech. Rep., 2021. [Online]. Available: <https://publications.csiro.au/publications/publication/PLcsiro:EP2021-2759>
- [3] R. Shaw, A. N. Espinosa, and L. Ochoa, "Dissemination Document "Low Voltage Networks Models and Low Carbon Technology Profiles";" Electricity North West Limited and The University of Manchester, Tech. Rep., 2015. [Online]. Available: <https://www.enwl.co.uk/globalassets/innovation/lvns/lvns-academic/summary-report.pdf>
- [4] C. H. Tam, F. Geth, and M. Nadarajah, "An inclusive model for a practical low-voltage feeder with explicit multi-grounded neutral wire," in *2022 IEEE Sust. Power Energy Conf.*, Perth, Australia, pp. 1–5.
- [5] W. Kersting, "The whys of distribution system analysis," *IEEE Industry Appl. Mag.*, vol. 17, no. 5, pp. 59–65, Sep. 2011.
- [6] S. Claeys, M. Vanin, F. Geth, and G. Deconinck, "Applications of optimization models for electricity distribution networks," *WIREs Energy Environ.*, vol. 10, no. 5, p. e401, Sep. 2021.
- [7] A. Urquhart, "Accuracy of low voltage electricity distribution network modelling," Ph.D. dissertation, School of Mech., Elect. and Manuf. Eng., Loughborough Univ., Leicestershire, 2016.
- [8] S. Claeys, F. Geth, and G. Deconinck, "Optimal power flow in four-wire distribution networks: Formulation and benchmarking," *Electric Power Sys. Res.*, vol. 213, p. 108522, Dec. 2022.
- [9] M. Vanin, F. Geth, R. D'hulst, and D. Van Hertem, "Combined unbalanced distribution system state and line impedance matrix estimation," *Int. J. Elect. Power Energy Syst.*, vol. 151, p. 109155, Sep. 2023.
- [10] W. H. Kersting, "Series impedance of overhead and underground lines," in *Distribution system modeling and analysis*, 3rd ed. Boca Raton, FL, USA: CRC Press, Jan. 2012, pp. 75–117.
- [11] J. R. Carson, "Wave propagation in overhead wires with ground return," *Bell Sys. Tech. J.*, vol. 5, no. 4, pp. 539–554, Oct. 1926.
- [12] A. J. Urquhart and M. Thomson, "Series impedance of distribution cables with sector-shaped conductors," *IET Gen. Transm. Distrib.*, vol. 9, no. 16, pp. 2679–2685, Dec. 2015.
- [13] H. Keshtkar, S. Khushalani Solanki, and J. M. Solanki, "Improving the accuracy of impedance calculation for distribution power system," *IEEE Trans. Power Del.*, vol. 29, no. 2, pp. 570–579, Apr. 2014.
- [14] A. Cristofolini, A. Popoli, and L. Sandrolini, "A comparison between Carson's formulae and a 2D FEM approach for the evaluation of AC interference caused by overhead power Lines on buried metallic pipelines," *PIER C*, vol. 79, pp. 39–48, 2017.
- [15] Y. Yuan, S. H. Low, O. Ardakanian, and C. J. Tomlin, "Inverse power flow problem," *IEEE Trans. Control Net. Syst.*, vol. 10, no. 1, pp. 261–273, 2023.
- [16] S. H. Low, "Reverse kron reduction of multi-phase radial network," 2024. [Online]. Available: <https://arxiv.org/abs/2403.17391>
- [17] Yizheng Liao, Y. Weng, Meng Wu, and R. Rajagopal, "Distribution grid topology reconstruction: An information theoretic approach," in *North Amer. Power Symp.* Charlotte, NC, USA: IEEE, Oct. 2015, pp. 1–6.
- [18] D. Deka, S. Backhaus, and M. Chertkov, "Estimating distribution grid topologies: A graphical learning based approach," in *Power Syst. Comput. Conf.* Genoa, Italy: IEEE, Jun. 2016, pp. 1–7.
- [19] I. Hiskens, "Power system modeling for inverse problems," *IEEE Trans. Circuits Syst. I: Regular Papers*, vol. 51, no. 3, pp. 539–551, Mar. 2004.
- [20] R. Cleenwerck, H. Azaioud, R. Claeys, T. Coosemans, J. Knockaert, and J. Desmet, "An approach to the impedance modelling of low-voltage cables in digital twins," *Electric Power Sys. Res.*, vol. 210, p. 108075, Sep. 2022.
- [21] W. H. Kersting, "Shunt admittance of overhead and underground lines," in *Distribution system modeling and analysis*, 3rd ed. Boca Raton, FL, USA: CRC Press, Jan. 2012, pp. 119–137.
- [22] F. Geth, R. Heidari, and A. Koirala, "Computational analysis of impedance transformations for four-wire power networks with sparse neutral grounding," in *Proc. ACM Int. Conf. Future Energy Syst.*, Virtual event, Jun. 2022, pp. 105–113.
- [23] A. R. Zubair and A. Olatunbosun, "Arithmetic and logical models of stranded transmission line conductors for voltage and voltage-drop analysis," *Int. J. Innov. Scient. Res.*, vol. 8, pp. 200–209, 2014.
- [24] "Standard for distribution line design overhead," Ergon Energy, Brisbane, Tech. Rep. STNW3361 Version 3, 2020.
- [25] "Standard for distribution line design underground," Ergon Energy, Brisbane, Tech. Rep. STNW3369 Version 2, 2019.
- [26] *IEC 60287-1-1 Electric cables - Calculation of the current rating - Part 1-1: Current rating equations (100% load factor) and calculation of losses - General*, Std., 2006.
- [27] R. C. Dugan and T. E. McDermott, "An open source platform for collaborating on smart grid research," in *2011 IEEE Power Energy Soc. General Meeting*. San Diego, CA: IEEE, Jul. 2011, pp. 1–7.
- [28] W. Kersting and W. Phillips, "Distribution feeder line models," *IEEE Trans. Ind. Applicat.*, vol. 31, no. 4, pp. 715–720, Aug. 1995.
- [29] *AS3607 Conductors: bare overhead, aluminium and aluminium alloy: steel reinforced*, Std., 1989.
- [30] *AS1746 Conductors—bare overhead—hard-drawn copper*, Std., 1991.
- [31] "Sector-shaped stranded aluminium, XLPE/PVC sheath 0.6/1kv to AS/NZS 4026." [Online]. Available: <https://goactive.nz/storage/media/2020/11/1605579763-a-ics-new-zealand-tds01-4calxl.pdf>
- [32] "NS220 overhead design manual," Ausgrid, Tech. Rep. [Online]. Available: <https://www.ausgrid.com.au/-/media/Documents/Technical-Documents/NS/NS220.pdf>
- [33] "Aerial catalogue," Nexans Olex, Tech. Rep. [Online]. Available: [https://www.voltimum.com.au/sites/www.voltimum.com.au/files/au/flipbooks/20120912-11\\_25\\_15/OLC12641\\_AerialCat.pdf](https://www.voltimum.com.au/sites/www.voltimum.com.au/files/au/flipbooks/20120912-11_25_15/OLC12641_AerialCat.pdf)